Motion/Force/Image Control of A Diagnostic Ultrasound Robot

W.-H. Zhu S. E. Salcudean† S. Bachmann P. Abolmaesumi

Dept. of Electrical and Computer Engineering
University of British Columbia
2356 Main Mall, Vancouver, BC
Canada V6T 1Z4

†Professor and Project Leader
(E-mail: tims@ece.ubc.ca)

Abstract

A fully counter-balanced 6-DOF robot for ultrasound carotid artery diagnosis has been developed in the Robotics and Control Laboratory at UBC [1]. This paper presents the controller design. The controller is basically a velocity controller capable of incorporating position control, force control, and image based control, in terms of shared control principle. Safety issue is deeply concerned in design of the control system. The fully counter-balanced mechanical design allows to use extremely small motor driving torques which result in 10N maximum force at the probe, and allows the probe to remain in its position in case of power failure. The robot can not only be positioned by Magellan device, setpoint automatic motion/force control, and image feature based control, but also be positioned by directly pushing its linkage in case that either the patient or the sonographer is at the slightest sign of discomfort. Feasibility experiments are reported.

1 Introduction

Ultrasound examination usually requires a sonographer to hold a probe in awkward positions for prolonged period of time. During the examination, the sonographer has to apply a pre-specified force while maintaining a stable position to achieve accurate and consistent measurements. This is because the contact force of the probe may result in skin deformation. Inconsistent contact force and position may affect the measurement accuracy significantly.

This special requirement has formed occupational hazard for sonographer [2, 3]. Prevalence of carpal tunnel syndrome and high incidence of musculoskeletal disorders have been reported [4].

Motivated by the need to alleviate these problems and to present a more ergonomic interface to the sonographer, a teleoperation system for carotid ultrasound diagnosis has been developed in the Robotics and Control Laboratory at UBC [1]. Compared to a digital teleultrasound system for transmitting ultrasound images previously developed by Sublett *et. al.* [5], this system allows the sonographer not only to view but also to manipulate the ultrasound transducer (probe) at the remote side. The ability to position the ultrasound transducer in response to acquired images would also be of benefit to image guided interventions and registration with past examination records or images obtained with other imaging methods, e.g. MRI. Furthermore, since the location of the ultrasound transducer can be determined via the forward kinematics of the robot, 3-D ultrasound images can be reconstructed from a series of 2-D image slices.

In addition to the general description of the teleoperated ultrasound robot system [1], this paper presents controller design in details. Section II gives a system overview. The controller design is addressed in section III. Section IV presents feasibility experiments. Conclusion is given by section V.

2 System Overview

The overall system is illustrated in Fig. 1. The system consists of a 6-joint robot, an ultrasound machine, a Magellan device, and three computers.

The robot with force sensor and ultrasound probe at its end-effector is fully counter-balanced in all six axes. A detailed drawing of the robot is illustrated in Fig. 2 [1] with probe frame shown in Fig. 3. A stage in the base is for forward (FWD) and Backward (BWD) motion. Two capstan drives are for up (UP) and down (DOWN), and left (LEFT) and right (RIGHT) motion. The position of the ultrasound probe is uniquely deter-

Table 1: Robot Robot specifications in Cartesian Space

Axis	**Ratio or Lead**	**Resolution**		**Equivalent**	**Maximum Force/Moment**	
Translation		(Theoretical)	(Experimental)	**Mass****	(Software)	(Hardware)
X	2.02 mm/rad	0.003 mm	< 0.1 mm	20.1 kg	10,0 N	129.9 N
Y	40:1	0.026 mm	< 0.2 mm	2.13 kg	9.0 N	15.5 N
Z	40:1	0.027 mm	< 0.2 mm	1.64 kg	9.0 N	15.5 N
Rotation						
Roll	93.6:1	0.0010°	$--$	0.63 kg·m^2	2.5 Nm	24.6 Nm
Pitch	50:1	0.0018°	$--$	0.68 kg·m^2	2.5 Nm	13.1 Nm
Spin	1:1	0.09°	0.09°	10^{-5} kg·m^2	0.15 Nm	0.18 Nm
Encoders	4000 CPR*	0.09°**				

* Cycles Per Revolution, ** Masses at zero positions.

mined by the first three axes, i.e. the stage and the two capstan drives. The orientation of the ultrasound probe is determined not only by the two capstan drives, but also by the roll, pitch, and spin axes. There are total three counter-weight. The ROLL counter-weight is adjusted such that the mass center of the arm linkage lies at the linkage plane. The ARM counter-weight is adjusted such that the mass center of the arm linkage lies at the axis of the DRIVE TOWER. Finally, the PENDULUM counter-weight is adjusted such that the mass center of the arm linkage plus capstan 2 lies at the axis of capstan 1. MAXON motors and US-DIGITAL encoders are used for current driving and position reading. JR^3 force sensor is attached at the end-effector for contact force measurement. The specifications of the robot is given by Table 1.

Fig. 1 Experimental setup of robotic ultrasound diagnosis0sis

Ultrasound machine USI-114B from Aloka Co. is used with probe UST-5512U-7.5.

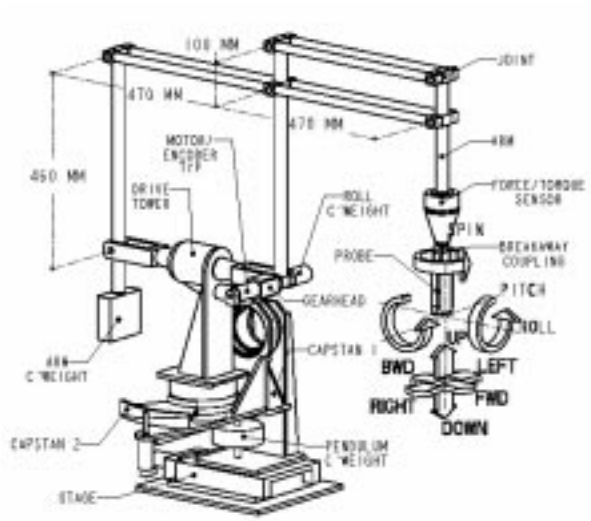

Fig. 2 The robot

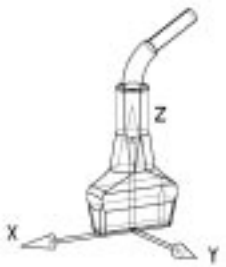

Fig. 3 The probe

A Magellan device from Logitech with 6-axis controllability is used as operational interface to the sonographer. It turns out that unilateral teleoperation is used since there is no active force feedback. Further research will replace the Magellan by PowerMouse [6, 7] to realize bilateral teleoperation [8].

Three computers consist of a host computer, a target computer, and an image processing computer. The host computer is a SUN Sparc Station running UNIX. It performs programs compilation, download to the target computer, and data display by StachoScope. Ethernet communication is used between the host computer and the target computer. The target computer is a Sparc 1E single board computer on VME Bus running VxWorks. It performs control calculations for the robot, including position/force reading, control algorithm calculation, output to motor amplifier, and communications with the host computer, the image processing computer, and the Magellan device. The image processing computer is a PC with Intel Pentium-II processor running Linux. It calculates ultrasound image feature data based on the algorithm develop by Abolmaesumi *et. al.* [9], and sends the image feature data to the target computer.

The system diagram is illustrated in Fig. 4.

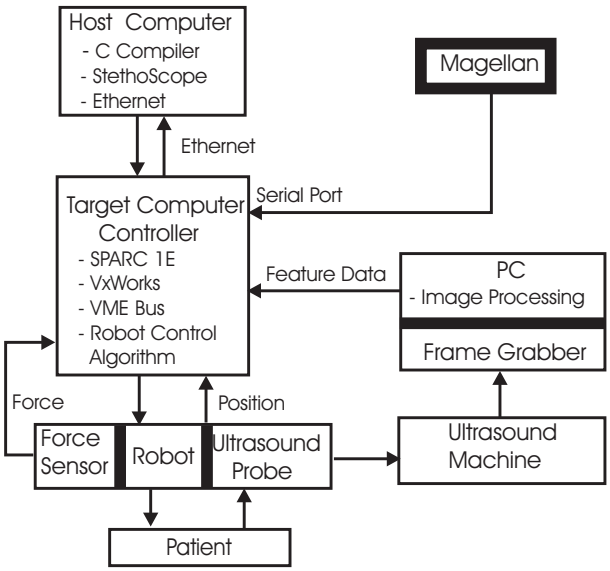

Fig. 4 System diagram

3 Controller Design

The controller diagram is illustrated in Fig. 5. The kernel of the controller is a velocity control loop which takes care of the robot dynamics including uncertainties and guarantees velocity asymptotic stability. Based on the velocity convergence where the actual velocity tracks the reference velocity asymptotically, position control, force control, and image feature servoing can all be incorporated by designing suitable reference velocity.

A. Robot Dynamics And Velocity Control Loop

The model for contact force between the ultrasound probe and the patient can be written as

$$F = \begin{cases} K_E \cdot (X - X_E) & \text{contact} \\ 0 & \text{non} - \text{contact} \end{cases} , \quad (1)$$

where $X \in R^6$ is the position/orientation of the probe, $X_E \in R^6$ is the contact position/orientation, and $K_E \in R^{6\times 6}$ is a symmetrically positive-definite stiffness matrix.

The robot dynamics is written as

$$M(\theta) \cdot \ddot{\theta} + d = \tau \ , \quad (2)$$

where $M(\theta) \in R^{6\times 6}$ is a symmetrically positive-definite inertial matrix with its diagonal elements listed in Table 1, $\theta \in R^6$ is the joint positions, $\tau \in R^6$ is the control torques, and $d \in R^6$ denotes disturbance forces including friction and contact force. The fully counter-balance mechanical design eliminates gravitational force. Meanwhile, the centripetal and Coriolis forces can be ignored since the robot is moving very slowly.

In view of (1), d can be expressed in terms of linear constant parameters as

$$d = Y(\theta, \dot{\theta})P \ , \quad (3)$$

where P is a constant parameter vector and Y is a corresponding regressor matrix.

The velocity control loop is designed as

$$\tau = K_\theta(\dot{\theta}_r - \dot{\theta}) + M(\theta)\ddot{\theta}_r + \hat{d} \ . \quad (4)$$

The first term in the right hand side is for feedback control, where $K_\theta \in R^{6\times 6}$ is symmetrically positive-definite. The second term is for feedforward compensation, and the third term is the output of the disturbance observer. The reference joint velocity $\dot{\theta}_r$ and acceleration $\ddot{\theta}_r$ are obtained by

$$\ddot{\theta}_r + C\dot{\theta}_r = CJ^{-1}V_r \ , \quad (5)$$

where $C = cI_6$ with $c > 0$, $V_r \in R^6$ denotes the reference velocity in Cartesian space, $J \in R^{6\times 6}$ is the invertible Jacobian matrix related to

$$V = J\dot{\theta} \ , \quad (6)$$

where $V \in R^6$ is the end-effector velocity in Cartesian space. Since the robot is moving very slowly, it is assumed throughout this paper that

$$\dot{J} \approx 0 \quad (7)$$

$$\dot{M}(\theta) \approx 0 \ . \quad (8)$$

Within a given interesting frequency range f_w, if $c > 2\pi f_w$, then it follows from (5) that

$$\dot{\theta}_r \approx J^{-1}V_r \ . \quad (9)$$

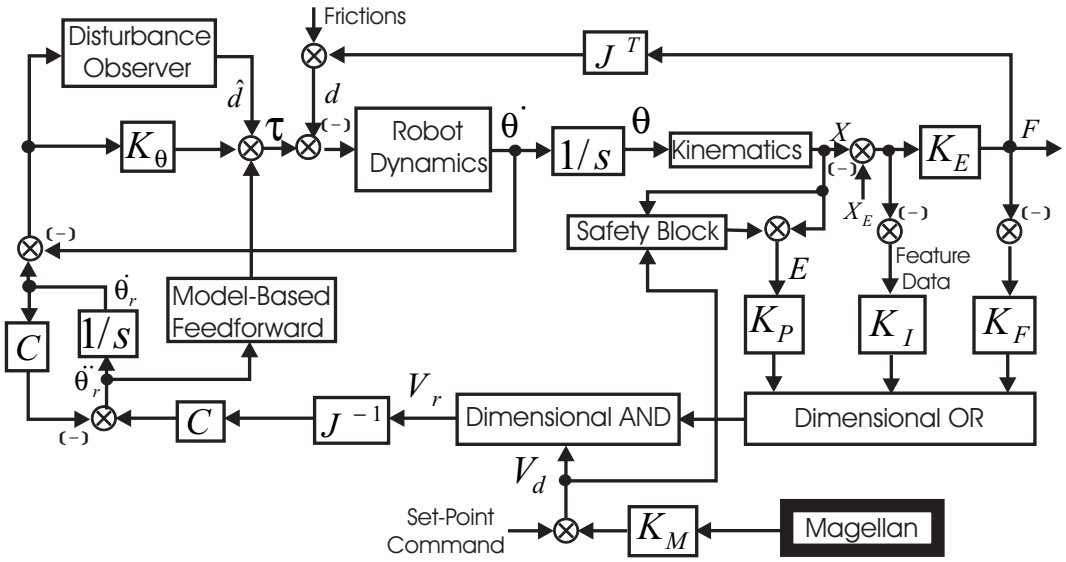

Fig. 5 Controller diagram

The disturbance observer is designed as

$$\hat{d} = Y(\theta, \dot{\theta})\hat{P} \,, \tag{10}$$

where $\hat{P}_i$, the ith element of $\hat{P}$, is estimated by using the $\mathcal{P}$ function defined in [10] as

$$\hat{P}_i = \mathcal{P}((\dot{\theta}_r - \dot{\theta})^T Y_i, \gamma_i, P_i^-, P_i^+) \,, \tag{11}$$

where Y_i is the ith column of $Y(\theta, \dot{\theta})$, $\gamma_i > 0$, P_i^- and P_i^+ denote the lower and upper bounds of P_i. In view of Lemma 1 in [10], it follows that

$$(P - \hat{P})^T [Y^T(\dot{\theta}_r - \dot{\theta}) - \Gamma^{-1}\dot{\hat{P}}] \leq 0 \tag{12}$$

with $\Gamma = diag\{\gamma_1, \gamma_2, \cdots, \gamma_i, \cdots\}$.

A non-negative function is chosen as

$$W = \frac{1}{2}\left[(\dot{\theta}_r - \dot{\theta})^T M(\theta)(\dot{\theta}_r - \dot{\theta}) + (P - \hat{P})^T \Gamma^{-1}(P - \hat{P})\right] \tag{13}$$

It follows from (2)-(4), (6), (8), (9), (10), and (12) that

$$\begin{aligned} \dot{W} &\leq -(\dot{\theta}_r - \dot{\theta})^T K_\theta(\theta)(\dot{\theta}_r - \dot{\theta}) \\ &\approx -(V_r - V)^T J^{-T} K_\theta J^{-1}(V_r - V) \,. \end{aligned} \tag{14}$$

This implies

$$V_r - V \in L_2 \bigcap L_\infty \,. \tag{15}$$

In case of $V_r \in L_\infty$, it follows from (5) and (9) that $\dot{V}_r \in L_\infty$. Furthermore, it follows from (2), (4), (6), and (7) that $\dot{V} \in L_\infty$. Finally, it follows that

$$V_r - V \longrightarrow 0 \,. \tag{16}$$

Asymptotic stability for velocity tracking is ensured.

B. Position/Force/Image Control

Since velocity tracking has been guaranteed by (16), position/orientation control, force control, and image feature servoing can all be accomplished by designing appropriate reference velocity V_r.

1) Position/Orientation Control: In position/Orientation, the reference velocity is designed as

$$V_r = V_d + K_P E \tag{17}$$

subject to

$$\int_0^t (V_d - V)^T K_P E dt \geq -\gamma^*, \tag{18}$$

where V_d denotes the desired velocity specified by set-point control and Magellan device, E denotes the position/orientation error, and $\gamma^* > 0$. Two examples given in [11] indicate that both position error in $SE(3)$ and orientation error in $SO(3)$ expressed with quaternion satisfy (18). In view of (15) and (18), it follows that

$$V_d - V \in L_2 \bigcap L_\infty \,, \tag{19}$$

$$E \in L_2 \bigcap L_\infty \,. \tag{20}$$

Furthermore, it yields

$$V_d - V \longrightarrow 0 \,, \tag{21}$$

$$E \longrightarrow 0 \,. \tag{22}$$

Asymptotic stability for position/orientation tracking is ensured.

2) Force Control: In force control, the reference velocity is designed as

$$V_r = V_d - K_F F \ , \tag{23}$$

where $K_F \in R^{6\times 6}$ is diagonal positive-definite. In view of (1) and (16), it follows that

$$\begin{aligned} V_r - V &= V_d - V - K_F F \\ &= V_d - V - K_F K_E (X - X_E) \\ &\rightarrow 0 \ . \end{aligned} \tag{24}$$

For constant V_d, it results in

$$F \longrightarrow K_F^{-1} V_d \ . \tag{25}$$

Force regulation is achieved.

3) Image Feature Servoing: Image feature servoing is to control the image feature point obtained by [9] to zero. Only X direction (see Fig. 3) is subject to image feature servoing. The corresponding reference velocity is designed as

$$(V_r)_1 = (V_d)_1 - K_I (X)_1 \ , \tag{26}$$

where $(\cdot)_1$ denotes the first element of $(\cdot)$, and $K_I > 0$. When $(V_d)_1 = 0$ (the first axis of Magellan device is disabled), image feature servoing

$$(X)_1 \longrightarrow 0 \tag{27}$$

can be achieved.

Dimensional OR operation is applied to all six dimensions. This means that the first axis can be either position/orientation control, force control, or image feature servoing. Each of the remaining five axes can be either position/orientation control or force control.

C. Safety Assurance

Different from industrial robots, safety issue is highly concerned with human centered robots which are directly dealing with human beings. In this system, the fully counter-balance mechanical design allows to use extremely small motor driving torques which are equivalent to maximum $10N$ at the end-effector, see Table 1. In case that either the patient or the sonographer is at the slightest sign of discomfort, the robot can be moved away directly by pushing its linkage with any force larger than $10N$. In order to prevent the robot from returning to the original position/orientation from there the robot is pushed away, a position tolerance ball is implemented as showed in Fig. 6.

For example, the actual robot position/orientation is changed from point B to point D by pushing its linkage. In order to prevent the robot from tracking its previous desired position/orientation at point A, the desired position/orientation is corrected from point A to point C. The radius of the position tolerance ball has to be larger than the maximum position/orientation error during normal operations to avoid undesired corrections.

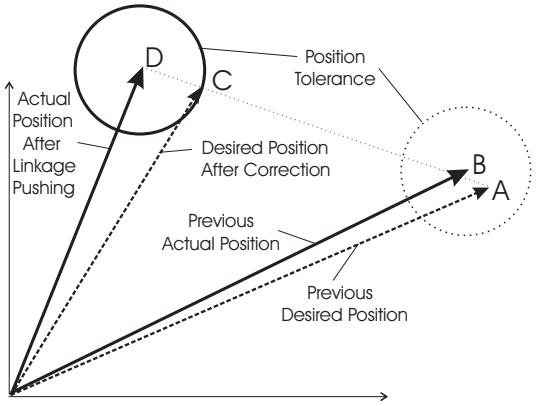

Fig. 6 Function of the safety block

4 Experiments

In the experiments, five sampling rates are used with the controller showing in Fig. 5: 500Hz is used in the velocity controller, including disturbance observer and feedforward compensation; 100Hz is used for kinematics calculations; 60Hz is used with StethoScope for data display in the host computer; and 25Hz and 10Hz are used for image feature data acquisition and Magellan data acquisition, respectively.

The experimental results are showing from Fig. 7 to Fig. 9. SI units are used in all plots. Fig. 7 shows free motion results. In the upper figure, the solid line represents the norm of desired linear velocity, while the dashed line represents the norm of position error. In the lower figure, the solid line represents the norm of desired angular velocity, while the dashed line represents the norm of orientation error expressed with quaternion. Zero position/orientation error is achieved in steady position/orientations.

Fig. 8 and Fig. 9 demonstrate motion/force control results in Z axis. The solid lines in the upper figure of Fig. 8 and in both figures of Fig. 9 represent the command signal. The dashed line in the upper figure of Fig. 8 represents a combination of velocity and force along the Z axis with $K_F = 0.006m/(sN))$. The lower figure of Fig. 8 shows the norm of position errors in X and Y axes. In Fig. 9, the dashed line in the upper figure represents the velocity, and the dashed line in the lower figure represents the contact force. After starting the procedure, a set-point command corresponds to $-0.024m/s$ or $-4.0N$ is given. Under this command, the robot approaches to the patient at a speed around

$-0.024m/s$. At about $t = 8.5s$, contact with the patient happens. The contact force approaches to $-4.0N$. At about $t = 16s$, Magellan command is added to the set-point command. The robot leaves the patient under the Magellan command at about $t = 21s$, and contacts with the patient again at about $t = 28.5s$. The upper figure of Fig. 8 verifies (24). In Fig. 9, the velocity tracks the command in free motion and goes to zero when contact happens. Instead, the force tracks the command in contact motion and tends to zero in free motion. These figures demonstrate very good velocity tracking in free motion and force tracking in contact motion.

By directly pushing the linkage with a force larger than $10N$, the robot can be moved to any place with the working space. After releasing the linkage, the robot comes back a bit of distance specified by the position tolerance ball (about $5mm$). Meanwhile, the robot maintains its position/orientation within the whole working space when electrical power turns off.

5 Conclusion

The controller design of a recently developed robot for carotid artery ultrasound diagnosis has been discussed in this paper. The inner control loop is basically a velocity controller which guarantees L_2 and L_∞ stability, and further asymptotic stability for velocity tracking. Based on this velocity controller, position/orientation control, force control, and image feature control can be easily incorporated with dimensional OR operation. The fully counter-balance mechanical design allows to use very small motor torques which enable either the patient or the sonographer to move the robot away easily by directly pushing its linkage, in case of discomfort. Feasibility experiments have been reported.

Acknowledgment

This work is supported by the Canadian IRIS Network of Centres of Excellence project SAL.

References

[1] S. E. Salcudean, G. Bell, S. Bachmann, W.-H. Zhu, P. Abolmaesumi, and P. D. Lawrence, "Robot-assisted diagnostic ultrasound - design and feasibility experiments," *MICCAI'99*, UK, 1999.

[2] M. Craig, "Sonography – an occupational health hazard?" *J. of Diagnostic Medical Sonography*, vol.1, pp.121-126, May/June, 1985.

[3] M. Craig, Occupational hazard of sonography: an update," *J. of Diagnostic Medical Sonography*, vol.6, pp.47-50, January/February, 1990.

[4] H. E. Vanderpool, E. A. Friis, B. S. Smith, and K. L. Harms, "Prevalence of carpal tunnel syndrome and other work-related musculoskeletal problems in cardiac sonographer" *J. of Occupational Medicine*, vol 35, pp.604-610, June, 1993.

[5] J. W. Sublett, B. J. Dempsey, and A. C. Weaver, "Design and implementation of a digital teleultrasound system for real-time remote diagnosis," *Proc. of 1995 Symposium on Computer-Based Medical Systems*, pp.292-298, 1995.

[6] S.E. Salcudean and N.R. Parker, "6-DOF Desk-Top Voice-Coil Joystick", 6th Annual Symposium on Haptic Interfaces for Virtual Environments and Teloperation Systems, Intl. Mech. Eng. Congr. Exp., DSC-Vol 61, pp.131-138, Dallas, Texas, Nov. 16-21, 1997.

[7] S.E. Salcudean, R. Six, R. Barman, S. Kingdon, I. Chau, D. Murray, and M. Steenburgh, "Control electronics and hybrid dynamic system-based API for a 6-DOF desktop haptic interface," Appears at The Winter Annual Meeting of The ASME, 1999.

[8] W.-H. Zhu and S. E. Salcudean, "Teleoperation with adaptive motion/force control," *Proc. of 1999 IEEE Int. Conf. Robotics and Automation*, vol.1, pp.231-237, 1999.

[9] P. Abolmaesumi, S. E. Salcudean, D. Lowe, and W.-H. Zhu, "Visual servoing for robot-assisted diagnostic ultrasound," Submitted to *2000 IEEE Int. Conf. Robotics and Automation.*

[10] W.-H. Zhu and J. De Schutter, "Adaptive control of mixed rigid/flexible joint robot manipulators based on virtual decomposition," *IEEE Trans. Robotics and Automation*, vol.15, no.2, pp.310-317, 1999.

[11] W.-H. Zhu, Y. G. Xi, Z. J. Zhang, Z. Bien, and J. De Schutter, "Virtual decomposition based control for generalized high dimensional robotic systems with complicated structure," *IEEE Trans. Robotics and Automation*, vol.13, no.3, pp.411-436, 1997.

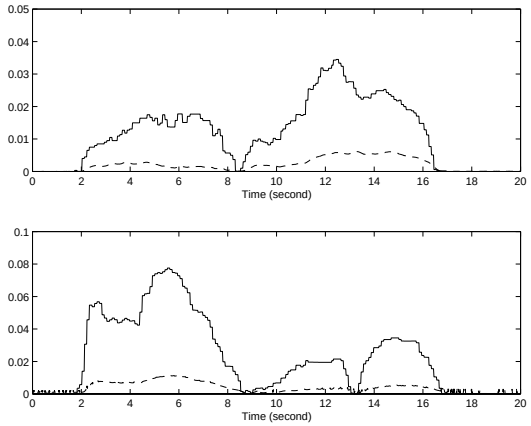

Fig. 7 Experimental result for position/orientation tracking in free motion

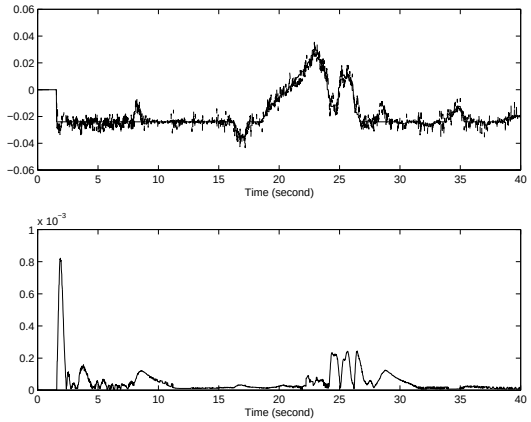

Fig. 8 Experimental result for motion/force control

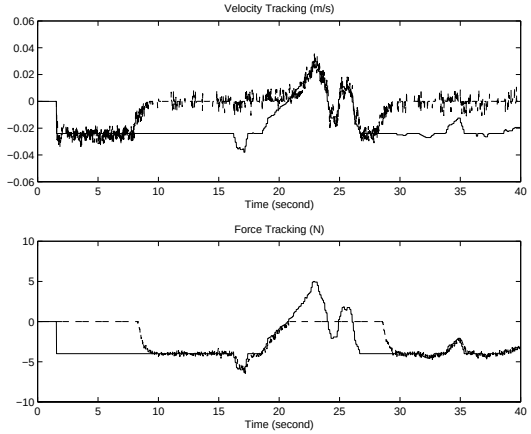

Fig. 9 Experimental result for velocity tracking and force tracking